UNIVERSITY OF PARDUBICE

FACULTY OF CHEMICAL TECHNOLOGY

Department of Graphic Arts and Photophysics

Amorphous chalcogenide thin films

Annotation of Ph.D. Thesis

Petra Hawlová

Pardubice, August 2017

Summary

This thesis focuses on the preparation and the study of some physico-chemical properties of selected bulk glass and thin films from Ge-As-Te system prepared by pulsed laser deposition. In order to determine of photo-induced changes, thin films with the composition $Ge_{10}As_{20}Te_{70}$, $Ge_{10}As_{30}Te_{60}$, $Ge_{10}As_{40}Te_{50}$, $Ge_{10}As_{50}Te_{40}$, $Ge_{10}As_{60}Te_{30}$ and $Ge_{20}As_{20}Te_{60}$ were exposed at 1064 nm, 1342 nm and 1550 nm. Thin films were also annealed below their glass transition temperature.

Scanning electron microscope with energy dispersive X-ray analyzer was used for the characterization of the morphology and chemical composition of the bulk glasses and thin films. The surface quality of thin films was evaluated by atomic force microscopy. The structure of bulk glasses and thin films was studied by Raman scattering spectroscopy. The glass transition temperature was assessed from differential scanning calorimetry data. Density and surface tension was determined for bulk glasses too. Laser desorption ionization time-of-flight mass spectrometry provided information about clusters created from bulk glasses of Ge-As-Te system by ionization of plasma plume generated by laser pulses. In prepared thin films, reversible and irreversible photoinduced phenomena were studied using variable angle spectroscopic ellipsometry.

The results show that promising composition, which showed photostable optical parameters (under exposure to radiation of wavelength 1064 nm, 1342 nm and 1550 nm) is $Ge_{20}As_{20}Te_{60}$. These thin films are potentially applicable in optics.

Aim of work

Amorphous chalcogenides are considered as advanced materials with many applications in different fields such as infrared optics, photonics, electronics, medicine, and environmental protection. Some potential applications of amorphous chalcogenides have been restricted due to instability of their optical parameters during light exposure. Photo-induced processes are typically linked with the changes of optical parameters, mainly the band gap energy and the refractive index.

Aim of this thesis is to find a photostable composition of amorphous chalcogenides from system Ge-As-Te.

Bulk materials were prepared by melt-quenching method and they were characterized and used for preparation of amorphous thin films by the pulsed laser deposition.

Thin films were characterized with emphasis to study their photostability by the spectroscopic ellipsometry.

Content

1. Introduction

Amorphous and glassy chalcogenides (AGC) based on S, Se and Te elements in combination with suitable element(s) from 14th or 15th group of the periodical system (typically Ge, As, etc.) are unique due to their photoinduced phenomena. Irradiation source of appropriate energy and intensity can change physico-chemical properties (refractive index, position of fundamental short-wavelength absorption edge, thickness, etc.) of amorphous chalcogenide thin films [1]. On the other hand, due to photoinduced changes of structure and properties, their potential applications in field of infrared optics, based on interesting nonlinear optical properties of amorphous chalcogenides have been limited [2].

On the basis of photoinduced phenomena knowledge in binary arsenic- and germanium-based amorphous chalcogenides [3-5], it would be supposed that in ternary Ge-As-Te (S, Se) materials, photodarkening (decrease of band gap energy) and photobleaching (increase of band gap energy), connected with positive or negative photorefraction (refractive index changes), could be compensated by an appropriate choice of composition. Nevertheless, the studies leading to optimization of intrinsic chemical composition of amorphous chalcogenides in order to prevent undesired photoinduced effects are rare [6-8], dealing with Ge-As-Se thin amorphous films. It is worthy to mention reported coexistence of fast photodarkening and slow photobleaching in thermally evaporated Ge-As-Se films [9, 10] as well as transient absorption effects induced by nanosecond pulsed lasers [11].

Based on interesting properties of bulk glasses and expectation of photostable thin films discovery, this work deals with amorphous thin films from Ge-As-Te system. These glasses have an excellent optical transparency in the 3–20 mm spectral window as well as large refractive index values (>3.5 at 1.55 mm) [12, 13]. In detail, the aim of this work is to find Ge-As-Te photostable thin films in as-deposited but preferably in relaxed (annealed) state. The term photostability can be defined as insensitivity of the material to light exposure in terms of constant values of refractive index and optical band gap.

2 Theoretical Part

2.1. Photoinduced phenomena

The photoinduced effects (PE) in AGC are strong and numerous. PE include changes of electronic and atomic structure, composition, phase and physico-chemical properties of chemical compounds induced by exposure of the material to light of appropriate energy and intensity. Photoinduced phenomena can be divided into irreversible and reversible [14]. Some photoinduced phenomena are shown in table 1.

Table 1 *Some photoinduced phenomena in S, Se and Te glasses. Irreversible PC are written in italics. Circles and squares represent the magnitudes (circles correspond to larger changes).*

	Photoinduced phenomena	S	Se	Te
Photon	*polymerization*	○	□	
	darkening	○	○	□
	fluidity	○		
	expansion	○	○	
Photo-thermal	anisotropy	○	○	
	crystallization	□	○	
Thermal	phase changes			○

Irreversible PE are found after exposure of as-deposited (virgin) AGC thin films. These thin films are unique in their structure, which cannot be recovered by any further processing of thin film. Irreversible PE include crystallization or amorphization process [15, 16], chemical reactivity [17], changes in refractive index [18], etc.

The structure and physico-chemical properties of AGC can also be changed reversibly. Reversible PE are crystallization-amorphization, changes of optical transmissivity, absorption edge shift, index of refraction, volume, etc. Reversible PE can be studied in bulk materials, annealed thin films, but they are not observed in the crystalline chalcogenides. The initial state can be restored by relaxation (annealing) at a temperature near glass transition temperature (Tg), usually for more than 60 minutes. While the photoinduced reversible changes occur mainly as photodarkening, reversible photobleaching is rare. [19]

2.2. Pulsed laser deposition

Thin chalcogenide films can be prepared by various methods. The pulsed laser deposition (PLD) is a useful technique for prepare thin films and is also suitable for the preparation of multilayers [20]. PLD can be considered as one of the simplest and most versatile methods for the preparation of thin films.

Scheme of PLD is shown in figure 1. The basis of the system is a vacuum chamber with holders of substrate(s) and target(s). The laser beam goes through a system of optical elements

(lenses, shutters, mirrors, laser window) to the vacuum chamber onto the target surface. Flexibility is a significant advantage of this arrangement, which allows the preparation of thin films with required physico-chemical properties. [14]
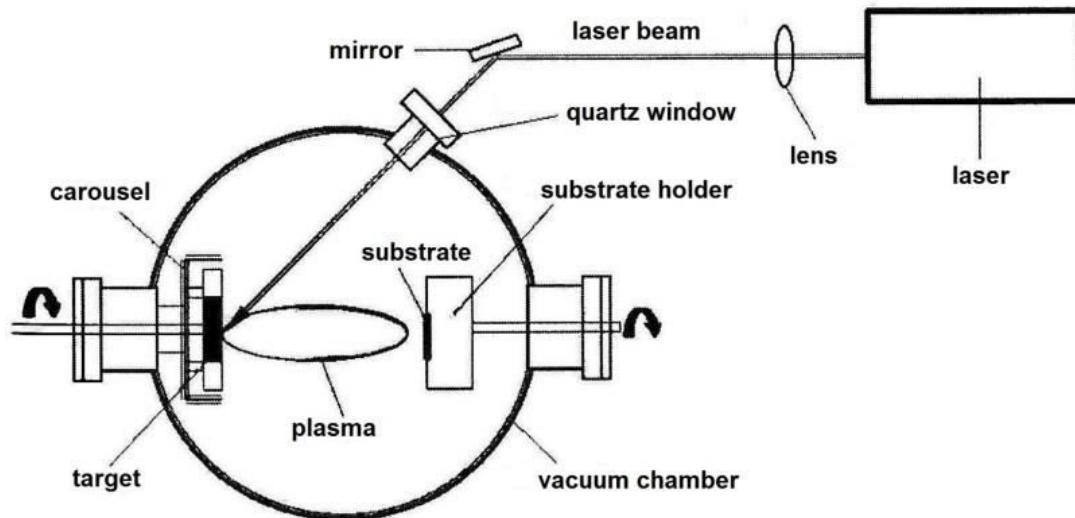

Figure 1 *Scheme of pulsed laser deposition system.*

PLD process uses for evaporation of solid-state materials gas-based excimer lasers (KrF), solid state lasers (e.g. Nd:YAG) or continuous lasers (CO_2). Laser pulses increase a temperature on a surface of target. The process is followed by melting and evaporation of target material from the surface and emission of the material to form the plasma ("plasma plume") which expands into vacuum. The plasma formed from the evaporated target material contains clusters of atoms and molecules, electrons, ions, fragments and microscopic particles of target material (solid or molten). The energy of pulses is sufficient to produce thin films (amorphous chalcogenides, metals, carbon, oxides and others).

The advantage of PLD is that process is almost stoichiometric. Each pulse evaporates thin surface layer, regardless of the vapour pressure of the individual components of the target material because the temperature of the target surface is higher than 3000 K [21]. PLD also has several disadvantages. High directivity plasma created in PLD is the first disadvantage; because of this phenomenon it is difficult to prepare thin films of uniform thickness over a larger area. This disadvantage can be solved in several ways: "off-axis" technique, PLD targets with rotation and displacement or rotation of the substrate by scanning the target with a laser beam, using targets with special geometry, possibly a combination of these methods [22].

2.3.   Ge-As-Te system

The potential applications of Ge-As-Te glasses are in the memory switches [23, 24]. The application of Ge-As-Te thin films can be for example as an optical data writing [25] or as NO_2 sensors [26].

The glass forming region of Ge-As-Te system is smaller than for the Ge-As-Se system [7] and depending on the way of cooling of the melt. When the melt is cooled on air, the glass forming region is divided into two parts (solid line), while cooling the melt in water results in a larger glass forming region (dashed line) [27, 28], as shown in figure 2. Studied compositions are also shown in the ternary diagram ($Ge_{10}As_{20}Te_{70}$, $Ge_{10}As_{30}Te_{60}$, $Ge_{10}As_{40}Te_{50}$, $Ge_{10}As_{50}Te_{40}$, $Ge_{10}As_{60}Te_{30}$ and $Ge_{20}As_{20}Te_{60}$). Compositions located in glass forming region with the same or similar representation of atomic percent as in previous studies [7, 29] were chosen for the study of photostability. Composition $Ge_{20}As_{20}Te_{60}$ (on the edge of the glass forming region) has been also included in the study, because the results of photostability study in Ge-As-Se system showed the best results for $Ge_{20}As_{20}Se_{60}$ composition.
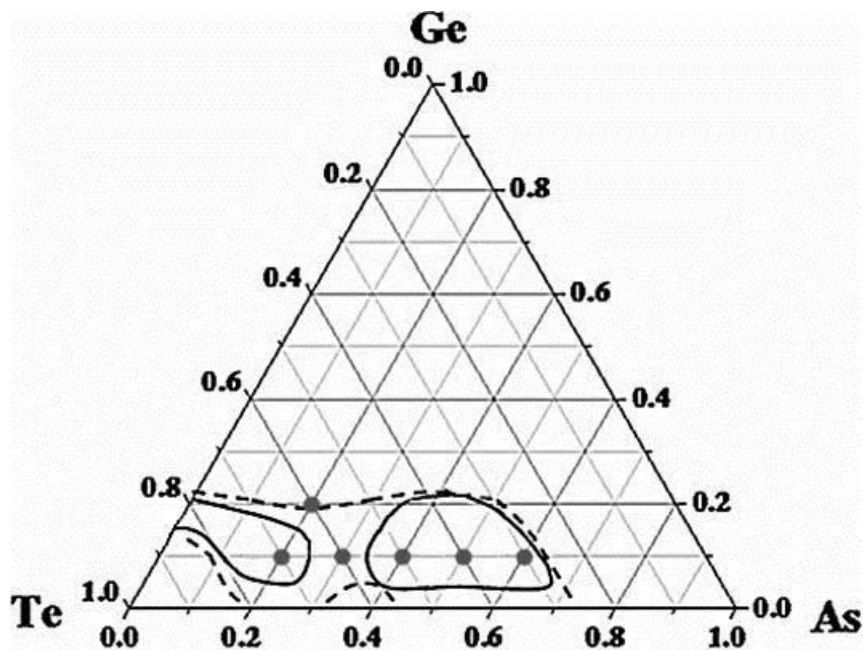

Figure 2 *Ternary diagram of Ge-As-Te system with glass forming region and studied composition [28]. Full curves are for cooling the melt on air. Dashed curves stand for cooling the melt in water. Grey spots correspond with the ternary compositions studied in this work.*

3. Experimental Part

3.1. Experimental procedures

Selected bulk samples from Ge-As-Te system ($Ge_{10}As_{20}Te_{70}$, $Ge_{10}As_{30}Te_{60}$, $Ge_{10}As_{40}Te_{50}$, $Ge_{10}As_{50}Te_{40}$, $Ge_{10}As_{60}Te_{30}$, and $Ge_{20}As_{20}Te_{60}$) were prepared by conventional melt and quench method. High purity elements (5–6N) were used for the synthesis. The synthesis (40 g batch) in evacuated and sealed silica ampoules was performed at 1050°C for 12 h in a rocking furnace (for the homogenization of the melt). After water quenching, the glass rods were annealed near, but below their glass transition temperatures for 2 h and slowly cooled down to room temperature (at 1°C/min). For physical properties measurements, polished samples of prepared materials were used.

For fabrication of thin films a KrF excimer laser operating in UV (248 nm) was used. The laser pulses had constant output energy of 300 ± 3 mJ per pulse, 30 ns pulse duration and 20 Hz repetition rate. The energy fluency was set at 2.6 $J.cm^{-2}$. Vacuum chamber (residual pressure <3.10^{-4} Pa) was used for the fabrication of thin films; substrates were chemically cleaned microscope glass slides and Si wafers. The substrates were positioned parallel to the target at target-tosubstrate distance of 5 cm. Off-axis PLD technique with rotating target and substrates was used to avoid deep damage of the target and to improve the thickness homogeneity of deposited thin films.

Photostability was studied with as-deposited and annealed thin films. The annealing was realized in inert atmosphere of pure argon; annealing temperature was 20°C below the respective glass transition temperature of the corresponding target glass. The duration of annealing was 120 min; the samples were consequently slowly cooled down to room temperature at $1°C.min^{-1}$. The photostability experiments were performed via exposure of thin films by laser sources operating at 1064 nm (1.17 eV), 1342 nm (0.92 eV) and 1550 nm (0.80 eV) with intensity of ~160 $mW.cm^{-2}$ for exposure time long enough (120 min) for the saturation of the photoinduced phenomena, if any. Laser exposures were realized in inert nitrogen atmosphere to avoid the oxidation of the films during the experiments.

3.2. Experimental techniques

A scanning electron microscope with energy-dispersive X-ray analyzer (SEM-EDS, JSM 6400-OXFORD Link INCA) was used for chemical composition determination of prepared bulk samples as well as Ge-As-Te thin films. SEM technique was also applied to observe the morphology of thin films using a field-emission gun SEM (JMS 6301F). X-ray diffraction (XRD) technique (D8-Advance diffractometer, Bruker AXS) was exploited to prove amorphous state of thin layers/bulk samples using Bragg–Brentano Ө–Ө geometry with CuKa radiation and secondary graphite monochromator. The diffraction angles were measured at room temperature from 5 to 65° (2Ө) in 0.02° steps with a counting time of 5 s per step.

The Raman scattering spectra of studied films were measured at room temperature by LabRAM HR spectrometer (Horiba Jobin-Yvon) with 785 nm laser as excitation source. The intensity of laser beam was kept at low level to avoid thermally induced structural transformations resulting from absorption of high laser power densities. The frequency resolution of used configuration was ~0.7 cm^{-1} per pixel.

Atomic force microscopy (AFM, Solver NEXT, NT-MDT) was used to study topography of Ge-As-Te thin films within typical scanned area 10 µm x 10 µm in semicontact mode.

Thermal analysis was performed with DSC 4000 instrument (PerkinElmer, Waltham, MA). The powders of bulk glasses (~10 mg) were heated at the rate of 10°C/min.

Optical functions (refractive indices and extinction coefficient spectral dependences) of bulk Ge-As-Te samples and thin films (here, also thicknesses were determined) were obtained from the analysis of spectroscopic ellipsometry data measured using an ellipsometer with automatic rotating analyzer (VASE, J.A. Woollam Co., Inc.). The measurement parameters are as follows: spectral region 300–2300 nm with 10 or 20 nm steps (depending on thickness of the films), angles of incidence 50°, 60° and 70°. For the analysis of VASE data we used Cody-Lorentz model [7], which includes the correct band edge function, weak Urbach absorption tail description as well as Lorentz oscillator function; this model is appropriate for the description of amorphous chalcogenides optical functions and their photo-induced changes [3].

Mass spectra were measured using either an AXIMA CFR or an AXIMA Resonance mass spectrometer equipped with a quadrupole ion trap mass analyzer (Kratos Analytical Ltd, Manchester, UK) and a time-of-flight mass analyzer. Using the AXIMA Resonance instrument, mass spectra were recorded in the ranges m/z 100–400, 250–1200, 800–3500, 1500–8000 and 3000–15000. Using the AXIMA CFR instrument, mass spectra were measured in the range m/z 100-2000. Both instruments used a nitrogen laser (337 nm) and delayed extraction. The laser energy was scaled in arbitrary units (a.u.) from 0 to 180; this relative scale will be used hereafter. The irradiated spot size was approximately 150 µm in diameter. The laser fluence was 1 J.cm^{-2}. All measurements were performed in both positive and negative ion reflectron mode. External mass calibration was performed using red phosphorus as a calibration standard in both ionization modes [30]. The experiments were performed in a repetition mode at a frequency of 5 Hz (10 Hz on AXIMA CFR) and with a pulse-time width of 3 ns. Each mass spectrum was obtained by the accumulation of spectra from at least 1500 laser shots.

Surface tension of bulk materials were measured by sessile drop method on CAM-100 (KSV). Liquids used for measurement were water, ethylene glycol, formamide and diiodomethane.

Density of bulk glasses were performed by hydrostatic method on balances ALS 220-4N (KERN) in toluene at temperature of 20 °C.

4. Results and discussion

Two series of $Ge_xAs_yTe_{100-x-y}$ thin films differing in thickness (~300 and ~1000 nm) were fabricated in order to satisfy criterion of penetration depth of the light sources used for the exposure experiments which must be equal or larger than the film thickness. The penetration depth for 1064 nm (1.17 eV) laser light was estimated to be 300–400 nm, laser beam of two other sources had penetration depth values larger than 2 mm. Because films with thickness around 300 nm were irradiated with 1064 nm (1.17 eV) and 1342 nm (0.92 eV) lasers and films with thickness around 1000 nm were exposed with 1342 nm (0.92 eV) and 1550 nm (0.80 eV) sources, above mentioned criterion was satisfied.

4.1. X-ray diffraction

Bulk Ge–As–Te samples were amorphous as confirmed by XRD data, excluding $Ge_{10}As_{60}Te_{30}$ material, which was partly crystalline (crystalline arsenic identified), and $Ge_{20}As_{20}Te_{60}$ sample (crystalline Te, $GeAs_2Te_4$, and $Ge_2As_2Te_5$ phases). Samples containing crystalline phase(s) were not used for further optical characterization. The thin films fabricated by PLD were amorphous according XRD patterns.

4.2. SEM-EDS & AFM

As determined using EDS, average chemical composition of fabricated bulk materials (measured at several points) is in good agreement with nominal one (Table 2). Large differences reported for $Ge_{10}As_{60}Te_{30}$ sample are due to the presence of very different crystalline phases. The SEM (Fig. 3) and AFM found smooth surface of thin films, without cracks and corrugations. We observed only rarely sub-micrometer sized droplets.
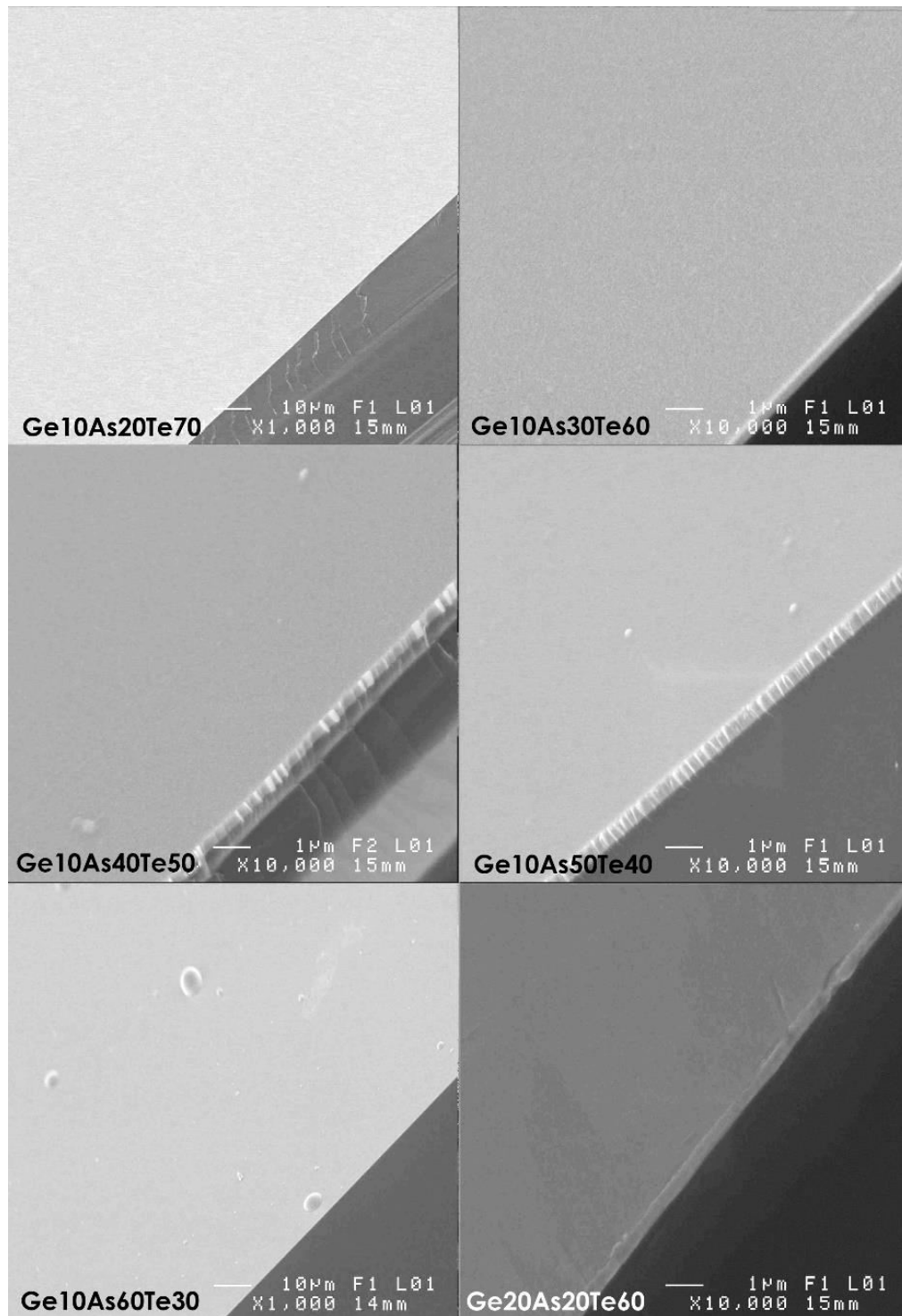
Figure 3 *Morphology of Ge-As-Te thin films by SEM.*

Surface roughness (RMS) values of all thin films determined by AFM were found to be lower than ~1.7 nm (Table 2); no changes in surface roughness were indicated for annealed, irradiated and post-annealing irradiated layers.

Table 2 *Nominal and real chemical composition from EDS (± 0.5 at. %) for bulk glasses and thin films of* $Ge_xAs_yTe_{100-x-y}$. *MCN stand for the mean coordination number calculated from nominal composition.*

Nominal composition	bulk/film	MCN	Ge (at. %)	As (at. %)	Te (at. %)	RMS (nm)
$Ge_{10}As_{20}Te_{70}$	bulk	2.4	9.6	18.3	72.1	
	film		13.3	23.0	63.7	1.72
$Ge_{10}As_{30}Te_{60}$	bulk	2.5	10.8	29.1	60.1	
	film		11.6	30.1	58.2	1.06
$Ge_{10}As_{40}Te_{50}$	bulk	2.6	9.8	39.2	51.0	
	film		12.2	38.6	49.2	1.05
$Ge_{10}As_{50}Te_{40}$	bulk	2.7	10.2	47.1	42.7	
	film		10.3	50.9	38.8	0.89
$Ge_{10}As_{60}Te_{30}$	bulk	2.8	10.4 - 24.1	21.9 - 57.1	32.5 – 54.0	
	film		14.1	46.0	39.9	1.08
$Ge_{20}As_{20}Te_{60}$	bulk	2.6	20.1	19.2	60.7	
	film		22.5	19.2	58.3	1.26

The chemical composition of fabricated layers, as determined by SEM-EDS, is in relatively good agreement with the composition of used bulk targets [13] (Table 2). The only exception is $Ge_{10}As_{60}Te_{30}$ composition, where the differences between thin film and bulk target composition are probably caused by non-homogeneity of the bulk material, which was partly crystalline. In spite of the fact that the bulk $Ge_{20}As_{20}Te_{60}$ target was completely crystalline (this composition is located on the border of the glass-forming region [28]), corresponding films were amorphous and their chemical composition agreed well with average composition of the used target.
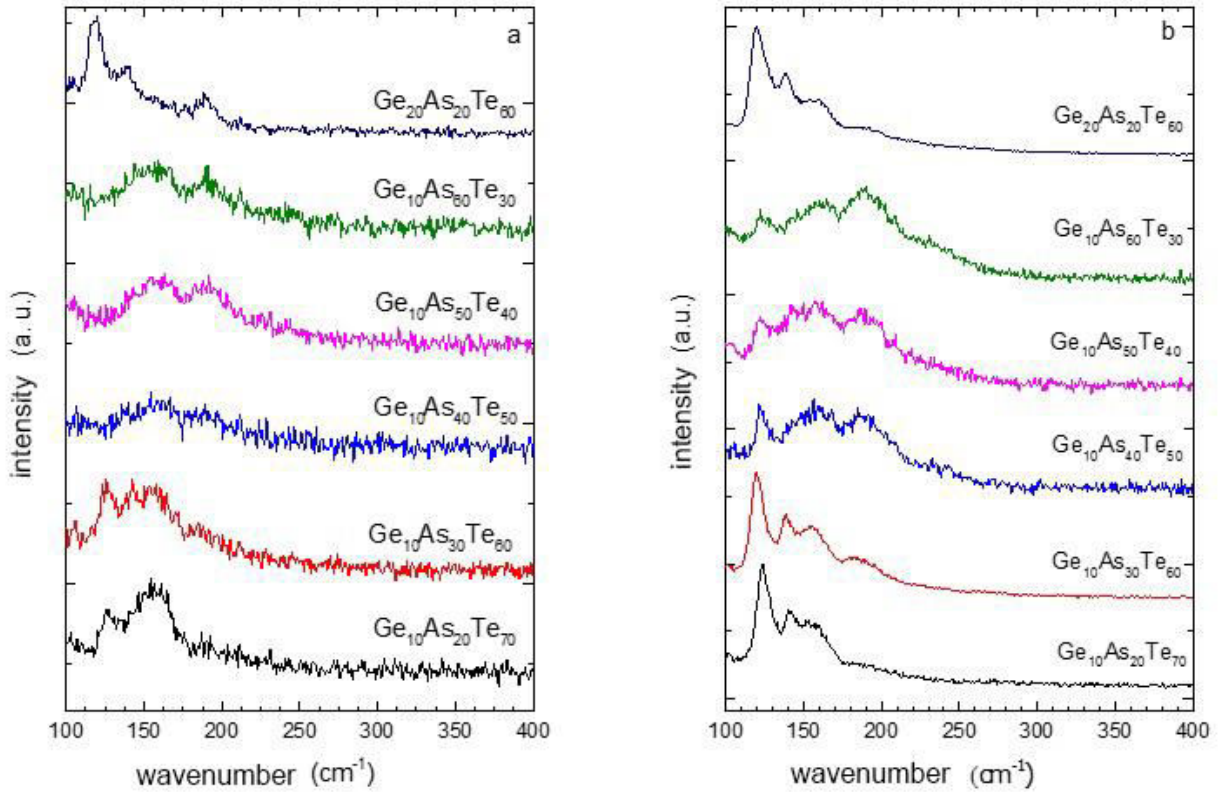
4.3. Raman scattering spectroscopy

Figure 4 *Raman scattering spectra of bulk materials (a) and as-deposited thin films (b) of Ge-As-Te system.*

The local structure of bulk materials, as-deposited, exposed, annealed and postannealing exposed Ge-As-Te films was studied via analysis of Raman scattering spectroscopy data. The examples of thin films' Raman spectra of bulk and corresponding as-deposited thin films of Ge-As-Te system are given in Fig. 4. In the measured Raman spectra, bands with maxima are located at ~123, ~141, ~159, ~,185–195 and ~220–230 cm^{-1}.

To have deeper insight into the structure of the Ge-As-Te bulk glasses and films, Raman scattering spectra for all states of the layers were measured. We discuss first the Raman spectra of bulk materials and as-deposited films illustrated in Fig. 4. Raman band peaking at ~123 cm^{-1} can be assigned to vibrations of $GeTe_4$ tetrahedra (A_1 symmetric stretching mode), $GeTe_{4-n}Ge_n$ (n = 1, 2) corner-sharing tetrahedra (A_1 mode) [30] and symmetric bending vibrations of $AsTe_3$ pyramids (A_1 mode) [31]. The Raman band with maximum at ~141 cm^{-1} could be attributed to vibrations of short Te disordered chains as in amorphous tellurium (experimentally observed at ~157 cm^{-1}), where the vibration frequency is shifted due to long range interaction between the chains [32]. The 141 cm^{-1} peak can be also connected with the E mode (antisymmetric stretching) in crystalline Te [31, 33]. It should be mentioned that the α-GeTe shows Γ_1 phonon mode at 140 cm^{-1} [34]. As the trigonal Te has the main Raman active A_1 symmetric stretching mode at 120 cm^{-1}, the Raman band at 123 cm^{-1} observed in Ge-As-Te films may have a mixed character with some contribution from Te–Te vibrations as well [31, 33]. The Raman band with maximum at ~159 cm^{-1} has been attributed to the

anti-symmetric bending vibrations of $AsTe_3$ pyramids (E mode) [31], A_1 mode of $GeTe_4$ edgesharing tetrahedral [30] and/or Te-Te vibrations as in amorphous tellurium (disordered chains) [32]. Further, we connect the Raman band peaking at ~185–195 cm^{-1} to A_1 mode of $GeTe_{4-n}Ge_n$ (n = 1, 2) edge-sharing tetrahedra vibrations [30]. We cannot exclude a contribution (to the band peaking at ~185–195 cm^{-1}) coming from vibrations of distorted octahedral $GeTe_3$ units in analogy with work of Voleská et al. [35]. Finally, very weak Raman band (shoulder) with maxima located at ~220–230 cm^{-1} can be associated with F_2 mode of $GeTe_{4-n}Ge_n$ tetrahedra anti-symmetric stretching vibrations [30]. In case of thin films with high arsenic content, it is necessary to take into account the presence of structural motifs rich in arsenic. Therefore we partly attribute the Raman bands peaking at 185–195 and ~220–230 cm^{-1} to symmetric (A_1 mode) and anti-symmetric (E mode) stretching vibrations of arsenic pyramids, respectively, in analogy with Ref [31].

Due to some differences in chemical composition of the bulk samples and thin layers, the Raman spectra of bulk samples and thin films of the same nominal composition showed a difference in amplitudes of some bands at identical wavenumbers (Figure 4).

The irradiation of as-deposited Ge-As-Te films has almost no effect on Raman spectra. The annealing of as-deposited layers leads to small decrease of amplitudes of Raman bands peaking at ~123 and 141 cm^{-1}. At the same time, amplitudes of Raman bands with maxima at ~159 and 185–195 cm^{-1} slightly increase. Depicted changes may be mainly connected with the slight increase of content of edge-sharing $GeTe_{4-n}Ge_n$ (n = 0, 1, 2) tetrahedra at the expense of corner-sharing ones. We cannot exclude that also some changes in ordering of short Te chains proceed on annealing. Post-annealing exposure leads to different effects. In case of films considered as photostable (Chapter 4.6., especially $Ge_{20}As_{20}Te_{60}$), no changes of Raman spectra were identified between annealed and post-annealing exposed states. On the other hand, films which are photosensitive present some changes in Raman spectra, qualitatively similar to changes on annealing (small amplitudes' decrease of bands peaking at ~123 and 141 cm^{-1}, slight increase of bands peaking at ~159 and 185–195 cm^{-1}). This observation leads to the conclusion that irradiation of relaxed, but photosensitive Ge-As-Te films reflects in structural changes regarding slight increase of content of edge-sharing $GeTe_{4-n}Ge_n$ (n = 0, 1, 2) tetrahedra at the expense of corner-sharing ones.

4.4.   DSC, density and surface tension

Results obtained from DSC, density and surface tension measurements are summarized and compared with mean coordination number in Table 3. The glass transition temperature (T_g) was not obtained for crystalline bulk material. Results for surface tension were analyzed by two methods. First, graphical method with linear regression was applied. Secondly, method exploiting two

equations with two unknowns was employed. Increased MCN is related only with increased T_g, other results seem not to show any relation with MCN.

Table 3 *Comparison of physico–chemical properties of fabricated Ge-As-Te bulk materials. Nominal and real mean coordination number, characteristic temperatures: T_g – glass transition temperature (* T_g of $Ge_{20}As_{20}Te_{60}$ composition was extracted from study of Krebs [28]), T_x – crystallization onset, T_c – crystallization temperature and T_m – melting temperature; density and surface tension estimated graphically and numerically.*

Composition	MCN		T_g	T_x	T_c	T_m	ρ	γ (mN/m)	
	teor.	real	(°C) ± 1°C				(g.cm^{-3})	gr. (R^2)	num.
$Ge_{10}As_{20}Te_{70}$	2.4	2.37	136	202	211	357	5.56 ±0.01	42.9 (0.89)	54.1
$Ge_{10}As_{30}Te_{60}$	2.5	2.51	155	196	203	366	6.13 ±0.12	41.8 (0.85)	54.6
$Ge_{10}As_{40}Te_{50}$	2.6	2.59	177	267	294	365	5.39 ±0.01	45.9 (0.90)	57.5
$Ge_{10}As_{50}Te_{40}$	2.7	2.67	196	314	326	409	5.32 ±0.01	43.1 (0.77)	61.7
$Ge_{10}As_{60}Te_{30}$	2.8	2.70-2.78	220	306	318	408	5.36 ±0.02	43.0 (0.84)	56.8
$Ge_{20}As_{20}Te_{60}$	2.6	2.59	185*	-	-	362	6.10 ±0.02	40.4 (0.75)	58.7

4.5.   LDI-TOF MS

LDI-TOFMS spectra of the Ge-As-Te powder samples were acquired in both positive and negative ion mode. The stoichiometry of the clusters detected in the plasma was determined via isotopic envelopes analysis and computer modelling. The mass spectra recorded using the AXIMA CFR and the AXIMA Resonance instruments were found to be similar.
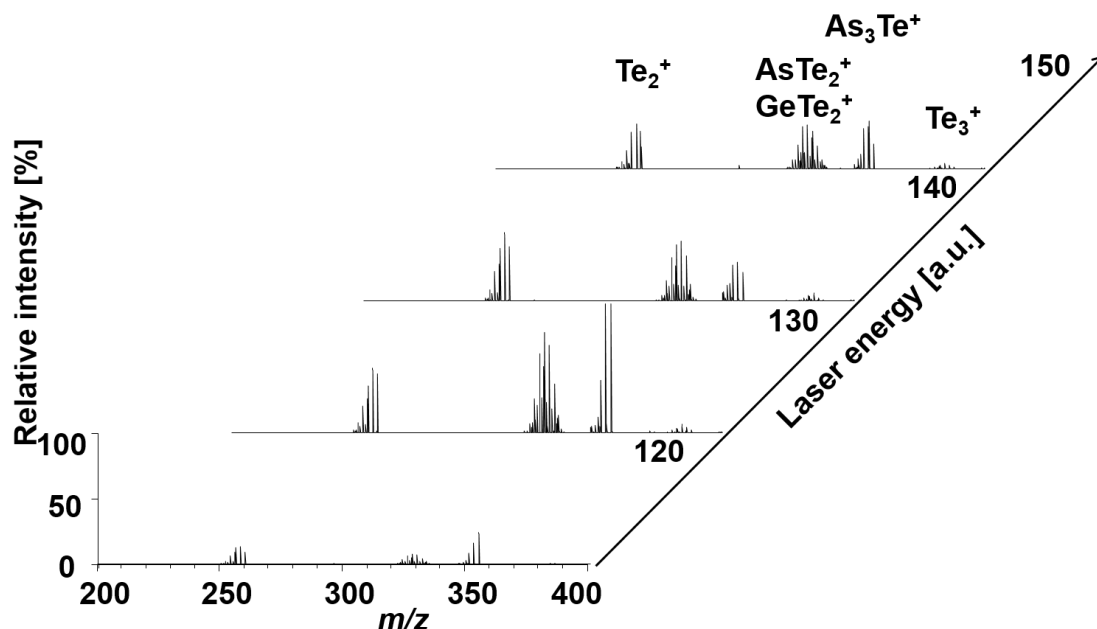
Positive ion mode

Figure 5 *The effect of laser energy on the LDI-TOF mass spectra of the $Ge_{10}As_{20}Te_{70}$ bulk sample. Conditions: positive ion reflectron mode, laser energy 120–150 a.u.; range m/z 200–400, relative intensity normalized to 600 mV.*

In the first instance the effect of the laser energy was studied and it was found that ionization begins at the laser energy of ~120 a.u. Figure 5 show the effect of laser energy on the mass spectra. At laser energy higher than 120 a.u., the intensities of the most of the peaks in mass spectra gradually decrease. This indicates that at higher laser energy the clusters decompose and thus the intensity of the peak corresponding to the Te^+ ion increases. The 'richest' spectra with the highest number of clusters and the highest peak intensities were observed at laser energy ~120–130 a.u., where the mass spectra show sufficient mass resolution and intensity of signals. The lowest mass peaks were identified as Te^+ and an overlap of the binary $Ge_2H_6^+$ and $GeAsH_{12}^+$ clusters (17 and 83% relative intensity). The other observed peaks at higher than m/z 200 were identified as Te_n^+ (n = 2–5), and overlap of the binary $AsTe_n^+$ and $GeTe_n^+$ clusters (n = 1–3). For example, for n = 1–2 overlap of $AsTe_n^+$ with $GeTe_n^+$ is observed (80 and 20%). Equal abundance was observed for n = 3, i.e. for the overlapping $AsTe_3^+$ and $GeTe_3^+$ clusters. In addition, binary As_3Te^+, $As_2Te_3^+$ and $AsTe_4^+$ clusters and a ternary $GeAsH_{12}^+$ one were identified. Although the Te_4^+ cluster is isobaric with the Ge_6As^+ cluster, the isotopic pattern observed is closer to Te_4^+ and formation of the Ge_6As^+ cluster is rather improbable when one takes into account the chemical composition of the materials. The

binary As_2Te^+ cluster was found to overlap with the ternary $GeAsTe^+$ one (58 and 42%) and the ternary $GeAsTe_2^+$ cluster was found to overlap with the tertiary $GeAsTe_2H_3^+$ one (8 and 92%). The most intense peak in the mass spectra was obviously the binary As_3Te^+ cluster. In the mass spectra related to the bulk $Ge_{10}As_{60}Te_{30}$ sample, the most intense peak observed corresponds to the overlap of the binary $AsTe_2^+$ and $GeTe_2^+$ clusters. The comparison of experimental and model mass spectra gives an excellent agreement.
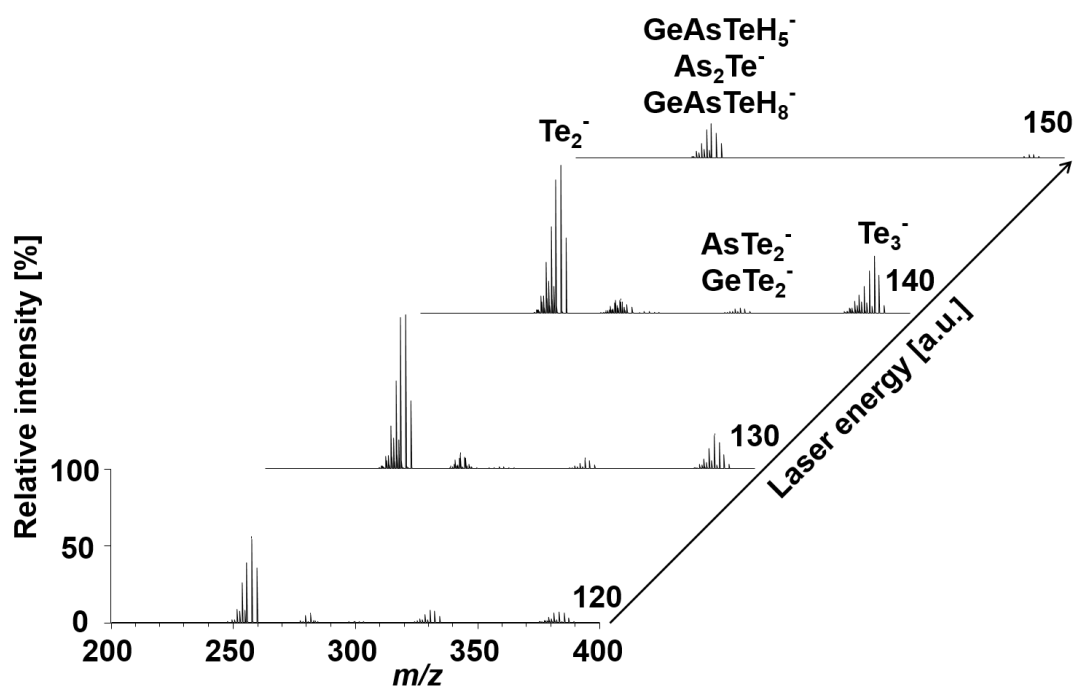
Negative ion mode

Figure 6 *The effect of laser energy on the LDI-TOF mass spectra of the $Ge_{10}As_{30}Te_{60}$ bulk sample. Conditions: negative ion reflectron mode, laser energy 120–150 a.u.; range m/z 200–400, relative intensity normalized to 2400 mV.*

The effect of the laser energy was also studied in this mode. It was found that ionization started at almost the same laser energy of ~120 a.u. as in positive ion mode. At higher laser energy (≥150 a.u.), the abundance of the clusters gradually decreased and some of the clusters, such as $GeAsTeH_5^-$, $GeAsTeH_8^-$ and $AsTe_2^-$, were no longer observed. This effect is shown in Fig. 6. In the case of $Ge_{10}As_{40}Te_{50}$ sample it was observed that with increasing laser energy the intensity corresponding to the Te_2^- cluster increased, while that of the $GeAsTeH_5^-$, $GeAsTeH_8^-$ and $AsTe_2^-$ clusters decreased or the clusters were not even detected. The same effect was also observed for other sample compositions. The 'richest' spectra with the highest number of clusters and the highest peak intensities were observed at a laser energy of ~120–130 a.u., as in positive ion mode. The following species were identified: Te_n^- (n = 1–4); and overlap of binary $AsTe_n^-$ and $GeTe_n^-$ clusters (n = 1–3). For example, for n = 1–2, overlap of $AsTe_n^-$ with $GeTe_n^-$ is observed (80 and 20%). Equal abundance was observed for n = 3, i.e. when $AsTe_3^-$ and $GeTe_3^-$ clusters overlapped. In addition, binary $Ge_2H_6^-$ was found to overlap with the ternary $GeAsH_6^-$ and $GeAsH_5^-$ clusters, with

relative abundances of 50, 10 and 40%. The ternary $GeAsTe_2^-$ cluster overlaps with the tertiary $GeAsTe_2H_3^-$ one (8 and 92%); overlap of the other binary As_2Te^- (16%) cluster with the tertiary $GeAsTeH_5^-$ (80%) and $GeAsTeH_8^-$ (4 %) ones was also detected. The most intense peak in the mass spectra for all Ge-As-Te samples is the Te_2^- cluster. The lowest peak intensities in the mass spectra were observed for the $Ge_{10}As_{50}Te_{40}$ material. The comparison of the experimental and theoretical mass spectra shows again very good agreement. An overview of the clusters observed in the mass spectra generated from Ge-As-Te samples in both, positive and negative ion mode is given in Table 4.

Table 4 *Summary of positively and negatively charged species in mass spectra of Ge-As-Te bulk materials. Letter z indicates number of tellurium atoms in the clusters, $^{+/-}$ indicates that the species were observed in both positive and negative ion mode. Note that the overlapping clusters (isobars) are given inside the () brackets.*

z	Clusters
0	$GeAsH_6^-$, $Ge_2H_6^{+/-}$, $GeAsH_5^-$, $GeAsH_{12}^+$
1	$Te^{+/-}$, $(AsTe^{+/-})$, $(GeTe^{+/-})$, $(GeAsTe^+)$, (As_2Te^+), $(GeAsTeH_5^-)$, (As_2Te^-), $(GeAsTeH_8^-)$, As_3Te^+
2	$Te_2^{+/-}$, $AsTe_2^{+/-}$, $GeTe_2^{+/-}$, $GeAsTe_2^{+/-}$, $GeAsTe_2H_3^{+/-}$
3	$Te_3^{+/-}$, $AsTe_3^{+/-}$, $GeTe_3^{+/-}$, $As_2Te_3^+$
4	$Te_4^{+/-}$, $AsTe_4^+$
5	Te_5^+

The series of $AsTe_n^{+/-}$ and $GeTe_n^{+/-}$ (n = 1–3) clusters show the continuous coordination of either arsenic or germanium with tellurium. For m/z values higher than 650, some carboncontaining impurities and oxidized arsenic $(As_yO_x)_n$ were observed, but no $Ge_xAs_yTe_z$ clusters were identified here.

LDI-TOF MS results might evidence at least some of structural units mentioned when analyzing Raman data. For example, $Te_n^{+/-}$ (*n*=2-4) and Te_5^+ clusters clearly confirm the presence of Te chains in the structure of Ge-As-Te materials. Further, evidence of $AsTe_3^{+/-}$, $AsTe_2^{+/-}$ or $AsTe^{+/-}$ clusters is coherent with the expected presence of $AsTe_3$ pyramids. In case of $GeTe_{4-n}Ge_n$ (*n*=0, 1, 2) tetrahedron, LDI-TOF MS detected probably fragments of such structural entities, namely $GeTe_3^{+/-}$, $GeTe_2^{+/-}$ or $GeTe^{+/-}$ clusters. Arsenic rich structural units could be represented in mass spectra by the presence of $As_2Te_3^+$, As_3Te^+ or $As_2Te^{+/-}$ clusters.

On the other hand, ternary or tertiary clusters identified in mass spectra of $Ge_xAs_yTe_z$ materials do not correspond with structural motifs observed by Raman spectroscopy and their origin is probably caused by reactions proceeding in plasma thanks to high energy of ions and clusters present in plasma plume.

Thus, the ions/clusters formed due to interaction of Ge-As-Te bulk materials with high energy laser pulses can resemble to certain extend the structure of original material. Because the stoichiometry of cluster ions formed did not change drastically when laser fluence was increased, it is therefore assumed (in agreement with the literature) that clusters are at least partially fragments of the original material. However, it is difficult to estimate to which extent LDI-TOF MS data account on actual structure (prior to desorption) but we are convinced that there is some relation.

4.6. Spectroscopic ellipsometry

The spectral dependencies of the refractive index of bulk Ge-As-Te samples (Figure 7) agree well with the ones of the corresponding thin layers; the $Ge_{20}As_{20}Te_{60}$ composition is not shown in the Figure 7 because the evaluation of the ellipsometric data for the crystalline sample is problematic. The prepared thin films show similar behavior of optical functions as the bulk samples of the same composition; this fact confirms the PLD technique is a proper method for thin film preparation.
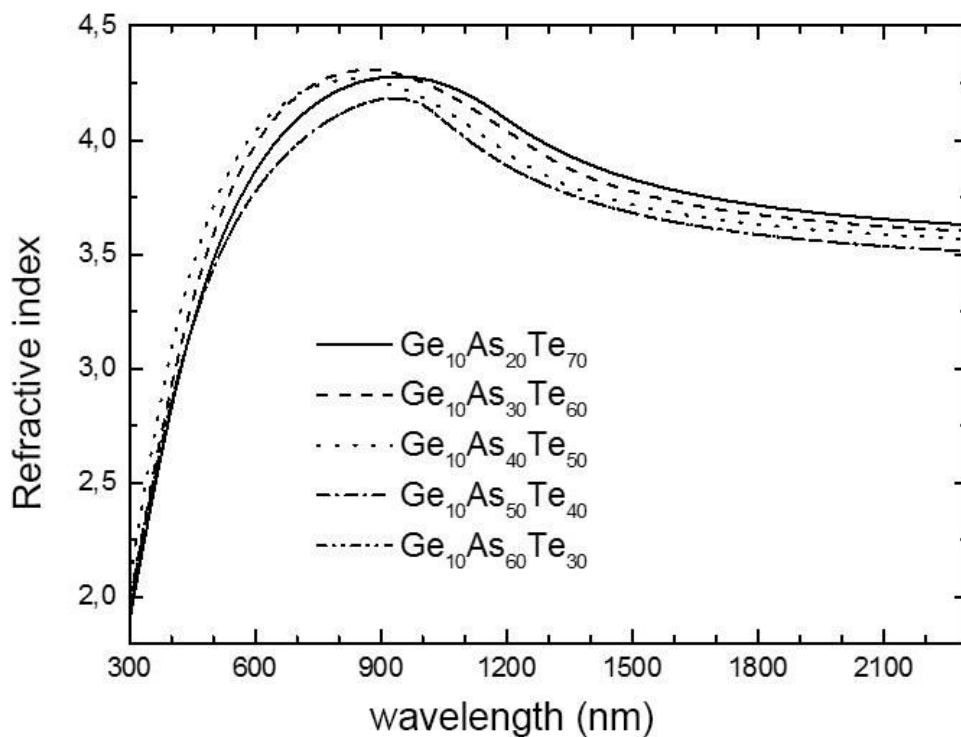

Figure 7 *Refractive indices spectral dependences (calculated from VASE data analysis, error in determination ± 0.01) for bulk samples of Ge-As-Te system.*

The thicknesses, optical band gap and refractive indices of all thin films were determined by VASE data analysis. The applicability of Cody-Lorentz model for the VASE data analysis of the films is confirmed by low values of mean square error (MSE) of the fitting procedure, typically MSE < 6.

Table 5 and 6 show optical band gap values and refractive indices at 1540 nm for 1000 nm PLD Ge-As-Te thin films in different states (as-deposited, exposed, annealed, post-annealing

exposed). The data presented stand for irradiation with laser sources operating at 1064 nm (1.17 eV, super band gap light) and 1342 nm (0.92 eV, band gap light). For clarity, data obtained for 1000 nm films, which were exposed with laser sources operating at 1342 nm (band gap light) and 1550 nm (0.8 eV, sub band gap light), are not shown in Tables 5 and 6. Examples of refractive indices spectral dependences are illustrated in Figure 8.
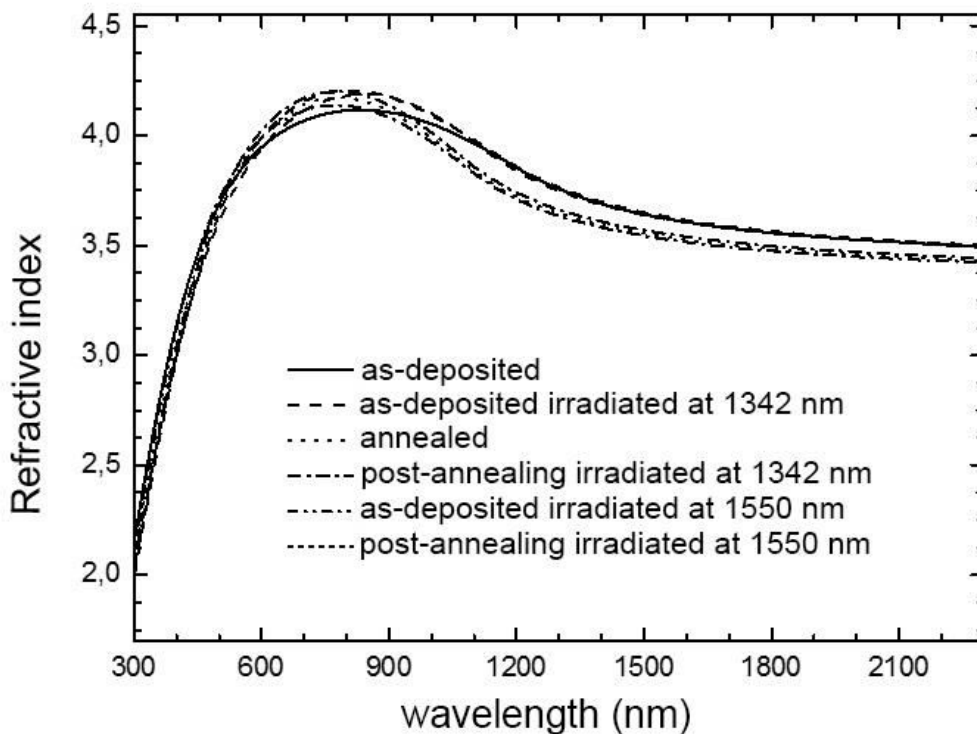

Figure 8 *Refractive indices spectral dependences (calculated from VASE data analysis, error in determination ± 0.01) for 1000 nm $Ge_{20}As_{20}Te_{60}$ thin film.*

From the obtained results, one can conclude that the irradiation of as-deposited Ge-As-Te layers leads to some photodarkening effect for ~300 nm thick films with nominal composition $Ge_{10}As_{20}Te_{70}$ (partly also $Ge_{10}As_{30}Te_{60}$); the photodarkening takes place for 0.92 eV irradiation (ΔE_g^{opt} up to ~0.11 eV). Under 1.17 eV exposure, films are photostable.

For ~1000 nm thick films, the impact of irradiation on as-deposited films has following trend. Under 0.92 eV irradiation, clear photobleaching was observed for most of the samples (ΔE_g^{opt} up to ~0.07 eV). On the other hand, under 0.8 eV irradiation, only weak photobleaching was detected for $Ge_{10}As_{40}Te_{50}$ and $Ge_{10}As_{50}Te_{40}$ layers (ΔE_g^{opt} up to ~0.04 eV), if any. Exposure of as-deposited Ge-As-Te films has generally only small effect on their refractive index values at 1540 nm, if any ($\Delta n \leq 0.02$).

The relaxation of as-deposited films via annealing in inert atmosphere generally results in their bleaching (ΔE_g^{opt} up to ~0.18 eV for $Ge_{10}As_{60}Te_{30}$), excluding 300 nm $Ge_{10}As_{20}Te_{70}$ layers which underwent darkening (ΔE_g^{opt} up to ~0.07 eV). The bleaching of as-deposited thin films due to annealing is connected with the decrease of refractive index (Δn up to ~0.16 in case of $Ge_{10}As_{60}Te_{30}$).

The behavior of relaxed (annealed) PLD Ge-As-Te amorphous thin films under exposure with different laser sources has not general trends (except the fact that no photobleaching was identified); that is why each composition will be commented separately. Two compositions ($Ge_{10}As_{50}Te_{40}$ and $Ge_{20}As_{20}Te_{60}$) exhibit almost completely photostable behavior of optical band gap in relaxed state. Relaxed $Ge_{10}As_{20}Te_{70}$ layers show photodarkening reaching ΔE_g^{opt} up to ~0.09 eV for 0.92 eV irradiation. Photodarkening was observed also for $Ge_{10}As_{30}Te_{60}$ relaxed films; ΔE_g^{opt} ~0.08 eV for 0.92 eV irradiation, magnitude of photodarkening is lower for two other irradiation sources. In case of $Ge_{10}As_{40}Te_{50}$ annealed films, photostability was found for 1.17 eV exposure; contrary, for 0.92 and 0.80 eV irradiation, weak photodarkening is reported. Finally, the photostability of $Ge_{10}As_{60}Te_{30}$ layers in relaxed state is rather good under 1.17 and 0.92 eV irradiation; however, under 0.80 eV exposure photodarkening with magnitude of ΔE_g^{opt} ~0.05 eV is seen. From the point of photorefraction, four studied compositions ($Ge_{10}As_{30}Te_{60}$, $Ge_{10}As_{40}Te_{50}$, $Ge_{10}As_{50}Te_{40}$ and $Ge_{20}As_{20}Te_{60}$) present almost zero photorefraction in relaxed state under all three irradiation sources.

Taking into account all the data, lowest values of photorefraction accompanied with lowest changes of band gap values were identified for $Ge_{20}As_{20}Te_{60}$ thin films, which are therefore considered as the layers with highest photostability among studied samples, especially in relaxed state. Zero photorefraction is of high importance for some applications of amorphous chalcogenides, such as for laser beam propagation in nonlinear regime [2]. That is why pulsed laser deposited $Ge_{20}As_{20}Te_{60}$ thin films are attractive and promising also due to their expected high (non)linear refractive index.

Discovery of thin films photostability in Ge-As-Te system, located at $Ge_{20}As_{20}Te_{60}$ composition (MCN = 2.6), is coherent with our earlier work dealing with Ge-As-Se amorphous layers, where the photostable composition was found to be $Ge_{20}As_{20}Se_{60}$ [7]. As pointed out by Calvez et al. [36], photostructural changes such as photodarkening decrease and tend to vanish in overcoordinated glasses, i.e. when MCN = 2.6 in Ge-As-Se system. In case of Ge-As-Te thin films studied here, some compositions have MCN higher than 2.6; however, they present some photoinduced phenomena. Moreover, $Ge_{10}As_{40}Te_{50}$ films having MCN = 2.6 are not completely photostable. Above mentioned facts lead to the conclusion that MCN does not seem to be the main decisive parameter influencing photostability of amorphous chalcogenides. Our conclusion is supported by the work of Khan et al., who studied light induced response of thermally evaporated Ge-As-Se thin films concluding that coexisting photodarkening and photobleaching do not show a regular trend with respect to MCN; instead evidence that Ge: As ratio plays important role, rather than rigidity of the amorphous network, is provided [10].

In an earlier work, Tanaka [37] claimed that the band gap (and super band gap) irradiation affects with higher efficiency lone pair electrons of chalcogen atoms (which are supposed to be responsible for photoinduced phenomena) than the sub band gap light. Our results do not correlate completely with this statement. Usually, changes of optical parameters are accompanied by structural changes. Generally, it is known that telluride films are easy to crystallize (which can also lead to changes in optical properties) in comparison with selenide/sulfide layers [38]. XRD patterns show that studied Ge-As-Te films are amorphous in different states of the samples (as-deposited, exposed, annealed and post-annealing exposed). Thus, no phase change of studied telluride thin films is observed under exposure/annealing.

Table 5 *Ge-As-Te thin films optical band gap values in different stages of the experiments (as-deposited, exposed, annealed and post-annealing exposed). Band gap values were extracted from VASE data analysis (± 0.01 eV). Note that data shown are for films with ~1000 nm thickness. E_{irr} is the energy of laser light used for irradiation experiments.*

E_{irr}	0.92 eV (1342 nm)				0.80 eV (1550 nm)			
	As- deposit.		Annealed		As- deposit.		Annealed	
Composition	Non-irra	Irra	Non-irra	Irra	Non-irra	Irra	Non-irra	Irra
$Ge_{10}As_{20}Te_{70}$	0.85	0.92	0.92	0.94	0.85	0.84	0.92	0.92
$Ge_{10}As_{30}Te_{60}$	0.88	0.93	0.92	0.93	0.88	0.88	0.93	0.88
$Ge_{10}As_{40}Te_{50}$	0.87	0.90	0.97	0.97	0.87	0.90	0.99	0.92
$Ge_{10}As_{50}Te_{40}$	0.88	0.93	1.02	1.02	0.88	0.92	1.00	0.99
$Ge_{10}As_{60}Te_{30}$	0.89	0.87	1.02	1.01	0.88	0.87	1.06	1.01
$Ge_{20}As_{20}Te_{60}$	0.89	0.95	1.00	1.00	0.89	0.90	1.02	1.01

Table 6 *Refractive indices (at 1550 nm) of Ge-As-Te thin films at different stages of the experiments (as-deposited, exposed, annealed and post-annealing exposed). Refractive indices were extracted from VASE data analysis (± 0.01). Note that data shown are for films with ~1000 nm thickness. E_{irr} is the energy of laser light used for irradiation experiments.*

E_{irr}	0.92 eV (1342 nm)				0.80 eV (1550 nm)			
	As- deposit.		Annealed		As- deposit.		Annealed	
Composition	Non-irra	Irra	Non-irra	Irra	Non-irra	Irra	Non-irra	Irra
$Ge_{10}As_{20}Te_{70}$	3.76	3.76	3.72	3.74	3.77	3.78	3.74	3.78
$Ge_{10}As_{30}Te_{60}$	3.72	3.72	3.66	3.66	3.72	3.71	3.67	3.69
$Ge_{10}As_{40}Te_{50}$	3.71	3.69	3.61	3.61	3.72	3.70	3.61	3.63
$Ge_{10}As_{50}Te_{40}$	3.68	3.66	3.57	3.57	3.68	3.67	3.58	3.60
$Ge_{10}As_{60}Te_{30}$	3.59	3.61	3.45	3.46	3.59	3.58	3.44	3.49
$Ge_{20}As_{20}Te_{60}$	3.62	3.62	3.54	3.53	3.63	3.63	3.55	3.55

It should be mentioned that a phenomenological description of the photoinduced effects in amorphous chalcogens and chalcogenides is often given by configuration-coordinate models [1, 37, 39], which propose the ground state of the system formed by a double-well potential with an energy barrier separating the ground and metastable states. After the photoexcitation, the system is transferred to the metastable state, where (after electronic relaxation), the electron and hole are trapped in the conduction-band tail state and in the valence-band edge state, respectively. In case that the distance between the electron and the hole is too long for immediate recombination, a polaron like structural change takes place. After the structural change, the carriers recombine and the structure is frozen, being more disordered. More disordered amorphous structure is connected with more random interlayer distances (van der Waals forces) leading to an increase of valence band broadening followed by the photodarkening and the refractive index rise.

Unfortunately, above mentioned configurational models cannot explain microscopic origin of the photoinduced effects resulting in volume changes. It is worthy to remind models of photoinduced volume changes proposed by Shimakawa [40], Tanaka [41] and Yang[42]. Shimakawa assumes macroscopic carrier diffusion and Coulomb repulsion among the layer fragments. Tanaka proposes the chalcogen atom bonds twisting with interlayer relaxation enhancing fluidity. Yang's model is based on bond angle increase and wrong bond creation. A model explaining both photoinduced expansion and contraction in both glassy and partly crystallized chalcogenides which involves Coulombic repulsive interaction (causing volume expansion) as well

as cross-linking of molecular units through bond-switching (leading to volume contraction) was introduced by Chen [43]. It should be noted that no general, quantitative model is available at present time. Nevertheless, as no clear trends in thicknesses changes of the Ge- As-Te films under irradiation were observed, we believe that the configuration-coordinate model is applicable in studied films. In order to better understand the phenomena observed in studied Ge-As-Te thin films, we envisage the measurements of transient photoinduced effects in near future.

5. Conclusions

In summary, pulsed laser deposition was exploited for the fabrication of Ge-As-Te amorphous thin films. Morphology of prepared films is of good quality and their surface roughness is low. Photostability of the layers was studied in as-deposited as well as annealed state of the samples under irradiation with lasers operating at 1064, 1342 and 1550 nm.

In studied Ge-As-Te thin films, no phase change occurs upon annealing/exposure as proved by XRD patterns. As observed by Raman scattering spectroscopy, the annealing/post-annealing exposure leads only to marginal structural effects, resulting in slight increase of edge-sharing $GeTe_{4-n}Ge_n$ (n = 0,1,2) tetrahedral content at the expense of corner-sharing ones. Laser desorption ionization time-of-flight mass spectrometry was employed for the analysis of the plasma formed from Ge-As-Te chalcogenide materials.

Mass spectra generated from Ge-As-Te powder samples are quite complex with several clusters overlapping. In positive ion mode, Te_n^+ (n = 1–5), $AsTe_n^+$ (n = 1–4), $GeTe_n^+$ (n = 1–3), As_nTe^+ (n=1–3), $As_2Te_3^+$, $GeAsTe^+$ and $GeAsTe_2^+$ entities were detected. In negative ion mode, Te_n^- (n = 1–4), $AsTe_n^-$ (n = 1–3), $GeTe_n^-$ (n = 1–3), As_nTe^- (n = 1–2) and $GeAsTe_2^-$ entities were identified. LDI-TOFMS also showed the presence of hydrogen/oxygen/carbon impurities in the studied materials leading to the formation of $Ge_2H_6^{+/-}$, $GeAsH_n^-$ (n = 5, 6), $GeAsH_{12}^+$, $GeAsTeH_n^-$ (n = 5, 8) and $GeAsTe_2H_3^{+/-}$ clusters and $(As_yO_x)_n$ entities.

Highest photostability connected with structural stability was found for $Ge_{20}As_{20}Te_{60}$ thin films, which are therefore promising for nonlinear applications.

6. References

[1] K. Shimakawa, A. Kolobov, and S. R. Elliott, Advances in physics 44 (1995) 475.

[2] M. Chauvet, G. Fanjoux, K.P. Huy, V. Nazabal, F. Charpentier, T. Billeton, G. Boudebs, M. Cathelinaud, and S. P. Gorza, Optics Letters 34 (2009) 1804.

[3] P. Nemec, V. Nazabal, and M. Frumar, Journal of Applied Physics 106 (2009) 023509.

[4] E. Sleeckx, L. Tichy, P. Nagels, and R. Callaerts, Journal of Non-crystalline Solids 200 (1996) 723.

[5] E. Vateva, Journal of Optoelectronics and Advanced Materials 9 (2007) 3108.

[6] G. Yang, H. S. Jain, A. T. Ganjoo, D. H. Zhao, Y. S. Xu, H. D. Zeng, and G. R. Chen, Optics Express 16 (2008) 10565.

[7] P. Němec, S. Zhang, V. Nazabal, K. Fedus, G. Boudebs, A. Moreac, M. Cathelinaud, and X.-H. Zhang., Optics Express 18 (2010) 22944.

[8] X. Su, R. Wang, B. Luther-Davies, and L. Wang, Applied Physics A 113 (2013) 575.

[9] P. Khan, A. R. Barik, E. M. Vinod, K. S. Sangunni, H. Jain, and K. V. Adarsh, Optical Express 20 (2012) 12416.

[10] P. Khan, H. Jain, and K. V. Adarsh, Scientific Reports 4 (2014)

[11] P. Khan, T. Saxena, H. Jain, and K. V. Adarsh, Scientific Reports 4 (2014) 6573.

[12] Z. Yang and P. Lucas, Journal of the American Ceramic Society 92 (2009) 2920.

[13] P. Hawlová, F. Verger, V. Nazabal, R. Boidin, and P. Němec, Journal of American Ceramic Society 97 (2014) 3044.

[14] P. Němec, ed., Příspěvek ke studiu chalkogenidových skel a amorfních chalkogenidových tenkých vrstev, Univerzita Pardubice, 2005.

[15] V. Lyubin, M. Klebanov, M. Mitkova, and T. Petkova, Journal of Non-Crystalline Solids 227 (1998) 739.

[16] V. I. Mikla and I. P. Mikhalko., Journal of Non-Crystalline Solids 180 (1995) 236.

[17] S. R. Elliot, Journal of Non-Crystalline Solids 81 (1986) 71.

[18] J. Teteris, Journal of Optoelectronics and Advanced Materials 4 (2002) 687.

[19] A. V. Kolobov, ed., Photo-induced metastability in amorphous semiconductors, Wiley-VCH GmbH and Co. KGaA, 2003.

[20] S. M. Green and e. al., PLD of thin films, J. Wiley, Intersci. Publ., New York, 1994.

[21] A. Gupta, PLD of thin films, J. Willey, Intersci. Publ., New York, 1994.

[22] M. Frumar , P. Němec , B. Frumarová, and T. Wágner, Vol. 2, INOE Publishing House, 2005.

[23] R. Pinto, Thin Solid Films 7 (1971) 391.

[24] S. Prakash, S. Asokan, and D. B. Ghare, Journal of Physics D: Applied Physics 29 (1996) 2004.

[25] R. M. Mehra, A. Pundir, A. Kapoor, and P. C. Mathur, Journal Optics 27 (1996) 139.

[26] S. Marian, D. Tsiulyanu, and H.-D. Liees, Sensors and Actuators B 78 (2001) 191.

[27] S. Sen, S. Soyer Uzun, C. J. Benmore, and B. G. Aitken, Journal of Physics: Condensed Matter 22 (2010) 405401 (9pp).

[28] H. Krebs and P. Fischer, Discussions of the Faraday Society 50 (1970)

[29] P. Hawlová, M. Olivier, F. Verger, V. Nazabal, and P. Němec, Materials Research Bulletin 48 (2013) 3860.

[30] K. Sladkova, J. Houska, and J. Havel, Rapid Communicaton in Mass Spectrometry, 23 [19] 3114–8 (2009).

[31] S. Sen, E. L. Gjersing, and B. G. Aitken, Journal of Non-Crystalline Solids 356 (2010) 2083.

[32] M. H. Brodsky, J. E. Smith, Y. Yacoby, and R. J. Gambino, Physica Status Solidi B-Basic Research 52 (1972) 609.

[33] A. S. Pine and G. Dresselhaus, Physical Review B 4 (1971) 356.

[34] E. F. Steigmeier and G. Harbeke, Solid State Communications 8 (1970) 1275.

[35] I. Voleska, J. Akola, P. Jovari, J. Gutwirth, T. Wagner, T. Vasileiadis, S. N. Yannopoulos, and R. O. Jones, Physical Review B 86 (2012)

[36] L. Calvez, Z. Y. Yang, and P. Lucas, Physical Review Letters 101 (2008) 177402.

[37] K. Tanaka, Photo-Induced Metastability in Amorphous Semiconductros, Wiley-WCH, Weinheim, 2003.

[38] M. Wuttig and S. Raoux, Zeitschrift für anorganische und allgemeine Chemie 638 (2012) 2455.

[39] A. V. Kolobov and K. Tanaka, Handbook of Advanced Electronic and Photonic Matterials and Devices 5 (2001)

[40] K. Shimakawa, N. Yoshida, A. Ganjoo, Y. Kuukawa, and J. Singh, Philosophical Magazine Letters 77 (1998) 153.

[41] K. Tanaka, Journal of Non-crystalline Solids 266 (2000) 889.

[42] C. Y. Yang, M. A. Paesler, and D. E. Sayers, Physical Review B 36 (1987) 9160.

[43] G. Chen, H. Jain, M. Vlcek, and A. Ganjoo, Physical Review B 74 (2006) 174203.

7. Publications by the author

7.1. Publications connected with the subject of the thesis

P. Hawlová, F. Verger, V. Nazabal, R. Boidin and P. Němec, Accurate Determination of Optical Functions of Ge–As–Te Glasses via Spectroscopic Ellipsometry, J. Am. Ceram. Soc. 97 (2014) 3044–3047.

P. Hawlová, F. Verger, V. Nazabal, R. Boidin and P. Němec, Photostability of pulsed laser deposited amorphous thin films from Ge-As-Te system, Scientific Reports 5, Article number 9310 (2015).

K. Šútorová, P. Hawlová, L. Prokeš, P. Němec, R. Boidin and J. Havel, Laser desorption ionization time-of-flight mass spectrometry of Ge-As-Te chalcogenides, Rapid Commun. Mass Spectrom. 29 (2015) 408–414.

P.Hawlová, R.Boidin, V.Nazabal, A.Moreac, L.Beneš, P.Němec: Photosensitivity of Ge-As-Te amorphous thin films fabricated by pulsed laser deposition. 6th International Symposium on Functional Materials, August 4-7, 2014, Singapore, Programme & Abstracts, p. 129.

P.Hawlová, V.Nazabal, L.Beneš, J.Holubová, Z.Černošek, J.Gutwirth, E.Černošková, M.Vlček, A.Moreac, P.Němec: Ge-As-Te bulk glasses: Physico-chemical properties and structure. 6th International Symposium on Functional Materials, August 4-7, 2014, Singapore, Programme & Abstracts, p. 259.

P.Hawlová, R.Boidin, V.Nazabal, L.Beneš, P.Němec: Photostability of pulsed laser deposited GexAsyTe100-x-y amorphous thin films. 6th International Conference Nanocon, November 5-7, 2014, Brno, Czech Republic, Conference Proceedings, p. 83.

M.Bouška, P.Hawlová, V.Nazabal, L.Beneš, P.Němec: Amorphous Ge-As-Te thin films prepared by Pulsed Laser Deposition – A photostability study. Photoptics 2015 – 3rd International Conference on Photonics, Optics and Laser Technology, March 12-14, 2015, Berlin, Germany, Conference Proceedings, p. 103.

7.2. Publications outside the subject of the thesis

P. Hawlová, M. Olivier, F. Verger, V. Nazabal and P. Němec, Photosensitivity of pulsed laser deposited $Ge_{20}As_{20}Se_{60}$ and $Ge_{10}As_{30}Se_{60}$ amorphous thin films, Materials Research Bulletin 48 (2013) 3860–3864.

I.Csarnovics, C. Cserhati, S. Kökényesi, M.R. Latif, M. Mitkova, P. Němec, P. Hawlová, T. Nichol, M. Veres, Light and electron beam induced surface patterning in Ge-Se system. J. Optoelectron. Adv. Mater. 18 (2016) 793-797.

I.Csarnovics, M. Veres, P. Němec, M.R. Latif, P. Hawlová, S. Molnar, S. Kokenyesi, Surface patterning in Ge-Se amorphous layers. J. Non-Cryst. Solids 459 (2017) 51-56.

P. Hawlová, M. Bouška, V. Nazabal, E. Baudet, Z. Černošek, P. Němec, Photostability of pulsed laser deposited As_xTe_{100-x} (x = 40, 50, 60) amorphous thin films. Opt. Lett. 42 (9) (2017) 1660-1663.

T.Syrovy, P,Janicek, J.Mistrik, K.Palka, P.Hawlova, L.Kubac, M.Klanjšek Gunde, Optical, electrical and morphological study of PEDOT: PSS single layers spiral-bar coated with various secondary doping solvents. Synt. Met. 227 (2017) 139-147.

V.Nazabal, M.Olivier, P.Hawlová, G.Boudebs, C.Focsa, M.Chauvet, G.Renversez, F.Verger, E.Baudet, P.Němec: Photosensitivity of pulsed laser deposited amorphous $(GeSe_2)_{100-x}(Sb_2Se_3)_x$ thin films. Materials Science & Technology 2013, October 27-31, 2013, Montréal, Canada, Final Program, p. 126.

G.Dascalu, O.G.Pompilian, I.Mihaila, S.Gurlui, P.Hawlová, P.Němec, V.Nazabal, C.Focsa: Pure and Rare-Earth Doped Gallium Lanthanum Sulphide Amorphous Thin Films Grown by Pulsed Laser Deposition in Various Temporal Regimes. E-MRS 2014 Spring Meeting, May 26-30, 2014, Lille, France, Conference Programme, J.VI 2.

G.Dascalu, O.Pompilian, N.Cimpoesu, V.Nazabal, P.Němec, P.Hawlová, B.Chazallon, S.Gurlui, C.Focsa: Improved surface structure and chemical composition of Ge-Sb-Te thin

films grown by femtosecond and picosecond PLD. E-MRS 2014 Spring Meeting, May 26-30, 2014, Lille, France, Conference Programme, JP.XI 33.

M.Olivier, R.Boidin, P.Hawlová, P.Němec, V.Nazabal: Kinetics of Photosensitivity in Ge-Sb-Se thin films. Photoptics 2015 – 3rd International Conference on Photonics, Optics and Laser Technology, March 12-14, 2015, Berlin, Germany, Conference Proceedings, p. 67.

P.Němec, V.Nazabal, E.Lavanant, P.Hawlová, Z.Černošek, E.Baudet: Photostability of amorphous As-Te thin films fabricated by pulsed laser deposition. EMN Meeting on Optoelectronics 2016, April 12-15, 2016, Phuket, Thailand, Program & Abstracts, p. 55-56.